Trigonal warping effect on velocity and transverse confinement length of topologically confined states in bilayer graphene

Diana A. Cosma* and Vladimir I. Fal'ko
Department of Physics, Lancaster University, LA1 4YB Lancaster, United Kingdom
(Received 7 August 2015; published 12 October 2015)

In bilayer graphene an interface between regions with opposite sign of the interlayer asymmetry gap leads to the spatial confinement of low-energy chiral modes [I. Martin, Y. M. Blanter, and A. F. Morpurgo, Phys. Rev. Lett. **100**, 036804 (2008)]. Here we study the influence of trigonal warping on the properties of the interface-guided stats and find that in the vicinity of the band edges the group velocity and transverse confinement length exhibit a nonmonotonic dependence on the crystallographic orientation of the crystal with respect to the interface.

DOI: 10.1103/PhysRevB.92.165412 PACS number(s): 85.75.−d, 75.47.Pq, 75.70.Ak

I. INTRODUCTION

Nontrivial properties of wave functions in electronic bands of some gapped materials (such as topological insulators [1] and superconductors [2]) lead to the existence of topologically protected interface/surface states inside the spectral gap of the bulk 3D or 2D material. Similar modes have been predicted to exist in asymmetrically biased bilayer graphene (BLG), in which a difference between the on-site energies on the two layers via a perpendicularly applied electric field induces an energy gap between the conductance and the valence bands [3–6]. The combination between the unusual properties of BLG and a topological defect, obtained by applying a potential difference with opposite sign in two regions of the flake, leads to the spatial confinement of the low-energy chiral modes in the gapped region and along the interface [7]. The robustness of these modes might significantly influence transport in BLG [8] which can have implications for graphene based valley filters [9] and valves [10].

In this paper we incorporate trigonal warping in the electron dispersion for a detailed analysis of the properties of the electron states confined along the interface between regions with opposite electric bias polarity. Such structures are, nowadays, feasible to produce using graphene encapsulated in hexagonal boron nitride with multiple split gates [11]. We find that in a BLG with trigonal warping the two modes inside the gap, found in the theory neglecting trigonal warping, persist even at small values of the gap. Our results show that trigonal warping only produces a strong dependance of the group velocity and the transverse confinement length of the interface states on the crystallographic orientation of the crystal.

II. MODEL

In BLG [3,5,12–15] the stacked layers have every A site within each layer surrounded by three B sites and vice versa, with intralayer coupling $\gamma_0 \sim 3$ eV; A_2 sites are on top of B_1 sites, with interlayer coupling $\gamma_1 \sim 0.4$ eV, while A_1/B_2 sites sit over/under the hexagons in the other layer and are coupled by "skew" hopping energy $\gamma_3 \sim 0.3$ eV. The low-energy properties of BLG can be described by the Hamiltonian with interlayer asymmetry gap [12,16]

$$\hat{H} = -\frac{v^2}{\gamma_1}\begin{pmatrix} 0 & \pi^{\dagger 2} \\ \pi^2 & 0 \end{pmatrix} + \xi v_3 \begin{pmatrix} 0 & \pi \\ \pi^\dagger & 0 \end{pmatrix} + \xi u(y)\left(\frac{1}{2} - \frac{v^2}{\gamma_1^2}\boldsymbol{p}^2\right)\sigma_z, \quad (1)$$

describing effective hopping between $A_1 - B_2$ sites. Here $u(z) = u \cdot \mathrm{sign}(z)$ [17] with $z = x\cos(\theta) + y\sin(\theta)$ and θ as the orientation of the interface with respect to the crystallographic direction of the crystal, $\xi = \pm 1$ for the two valleys, v is the Fermi velocity, $v_3 = \frac{\sqrt{3}a\gamma_0}{2\hbar}$ with $a = 2.46$ Å as the lattice constant, $\pi = p_x + ip_y$ parametrizes the in-plane momentum relative to the Brillouin zone (BZ) corners, $\boldsymbol{K}$ and $\boldsymbol{K}'$ with $\boldsymbol{p}^2 = p_x^2 + p_y^2$, and σ_z is the Pauli matrix.

The first term in Eq. (1) describes the low-energy electronic states which reside on the sites A_1 and B_2 and form two approximately parabolic bands that touch each other at the $\boldsymbol{K}$ and $\boldsymbol{K}'$ points. The second term incorporates the "skew" hopping which induces a trigonal warping (TrW) effect and splits the parabolic bands into four pockets which merge together at energy $\epsilon_{TW} \approx \frac{\gamma_1}{4}(\frac{v_3}{v})^2$. Finally, the last term in the above equation contains the interlayer asymmetry $u(y)$ (which preserves the electron-hole symmetry and leads to the opening of a gap [5] in the spectrum) as well as the influence of the high-energy states, $-\frac{v^2}{\gamma_1^2}\boldsymbol{p}^2$, which reside on A_2 and B_1 sites, form the split bands, and give the dispersion a "Mexican hat"-like shape.

On both sides of the interface the spectrum has the form

$$E = \pm\sqrt{\alpha^2\boldsymbol{p}^4 + \beta^2\boldsymbol{p}^2 - \alpha\beta\left(2p_x^2 - 6p_x p_y^2\right) + u^2\left(\frac{1}{2} - \frac{v^2}{\gamma_1^2}\boldsymbol{p}^2\right)^2},$$

$$\alpha = \frac{v^2}{\gamma_1}, \quad \beta = \xi v_3,$$

illustrated in Fig. 1. For $u \leqslant 5$ meV, the second and third terms in the Hamiltonian dominate at low energies, and the spectrum exhibits four clearly defined pockets in the vicinity of the gap, as shown by the isoenergetic lines in Fig. 1 (left panel). For 5 meV $< u <$ 40 meV, the interlayer asymmetry competes with TrW causing a lowering of the side pockets shown in Fig. 1 (central panel), whereas the central pocket remains unchanged. Finally, for $u \geqslant 40$ meV the last term in

*d.cosma@lancaster.ac.uk

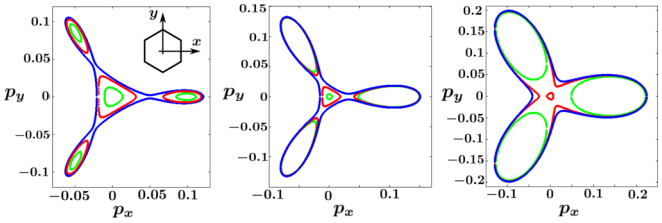

FIG. 1. (Color online) Isoenergetic lines for gaps $u = 2$ meV (left panel), 20 meV (central panel), and 50 meV (right panel) and $\theta = 0$. The colors distinguish the isoenergetic lines at different energies as follows: left panel $\epsilon = 1.1$ meV (green), 1.3 meV (red), and 1.4 meV (blue); central panel $\epsilon = 10.001$ meV (green), 10.01 meV (red), and 10.02 meV (blue); right panel $\epsilon = 24.9$ meV (green), 24.999 meV (red), and 25.02 meV (blue).

Eq. (1) becomes just as strong as the TrW effect which leads to the conversion of the central pocket into a saddle point located above the Lifshitz transition energy, as depicted in Fig. 1 (right panel), at which the isoenergetic lines reconnect.

III. CONFINEMENT OF LOW-ENERGY ELECTRON STATES

In the absence of TrW, the eigenvectors of the Hamiltonian in Eq. (1) are of the form

$$\Psi^{\pm}(y) = \sum_{i=1}^{4} \frac{A_i^{\pm}}{\sqrt{v_i^{\pm}}} \begin{pmatrix} 1 \\ \alpha_i^{\pm} \end{pmatrix} e^{\lambda_i^{\pm} y},$$
$$\alpha_i^{\pm} = \frac{-\left(\frac{v^2}{\gamma_1} + \eta\frac{v_3}{v}\right)(p_x + \lambda_i^{\pm})^2 + \xi v_3 (p_x - \lambda_i^{\pm})}{\xi u(y)\left(\frac{1}{2} - \frac{v^2}{\gamma_1^2}\left(p_x^2 + \lambda_i^{\pm 2}\right)\right) + E}, \tag{2}$$

above $y > 0$ (+) and below $y < 0$ (−) the interface. Here $A_i^{\pm}$ are the wave amplitudes, $\lambda_i^{\pm} = i p_{y_i}^{\pm}$ are the momenta perpendicular to the interface, $v_i^{\pm} = |\partial E/\partial p_y^{\pm}|$ is the group velocity, and i labels the four components of the wave function. The amplitudes A_i^{+} and A_i^{-} on the two sides of the interface can be matched,

$$\begin{pmatrix} A_1^+ \\ A_2^+ \\ A_3^+ \\ A_4^+ \end{pmatrix} = T \begin{pmatrix} A_1^- \\ A_2^- \\ A_3^- \\ A_4^- \end{pmatrix}, \tag{3}$$

using the transfer matrix [18] $T = N^{-1}M$. To build this matrix we employed the continuity of the electron wave function $\Psi(0)^+ = \Psi(0)^-$ and its derivative $\partial\Psi(0)^+/\partial y = \partial\Psi(0)^-/\partial y$ at $y = 0$, and found that

$$M = \begin{pmatrix} 1 & 1 & 1 & 1 \\ \alpha_1^+ & \alpha_2^+ & \alpha_3^+ & \alpha_4^+ \\ \lambda_1^+ & \lambda_2^+ & \lambda_3^+ & \lambda_4^+ \\ \alpha_1^+\lambda_1^+ & \alpha_2^+\lambda_2^+ & \alpha_3^+\lambda_3^+ & \alpha_4^+\lambda_4^+ \end{pmatrix} \times \begin{pmatrix} \frac{1}{\sqrt{v_1^+}} & 0 & 0 & 0 \\ 0 & \frac{1}{\sqrt{v_2^+}} & 0 & 0 \\ 0 & 0 & \frac{1}{\sqrt{v_3^+}} & 0 \\ 0 & 0 & 0 & \frac{1}{\sqrt{v_4^+}} \end{pmatrix},$$
$$N = \begin{pmatrix} 1 & 1 & 1 & 1 \\ \alpha_1^- & \alpha_2^- & \alpha_3^- & \alpha_4^- \\ \lambda_1^- & \lambda_2^- & \lambda_3^- & \lambda_4^- \\ \alpha_1^-\lambda_1^- & \alpha_2^-\lambda_2^- & \alpha_3^-\lambda_3^- & \alpha_4^-\lambda_4^- \end{pmatrix} \times \begin{pmatrix} \frac{1}{\sqrt{v_1^-}} & 0 & 0 & 0 \\ 0 & \frac{1}{\sqrt{v_2^-}} & 0 & 0 \\ 0 & 0 & \frac{1}{\sqrt{v_3^-}} & 0 \\ 0 & 0 & 0 & \frac{1}{\sqrt{v_4^-}} \end{pmatrix}.$$

Assuming that in Eq. (3) the amplitudes A_1^-, A_2^-, A_3^+, A_4^+ are the ones corresponding to wave function components which diverge away from the interface ($e^{\lambda_i^{\pm} y} \to \infty$), we substitute

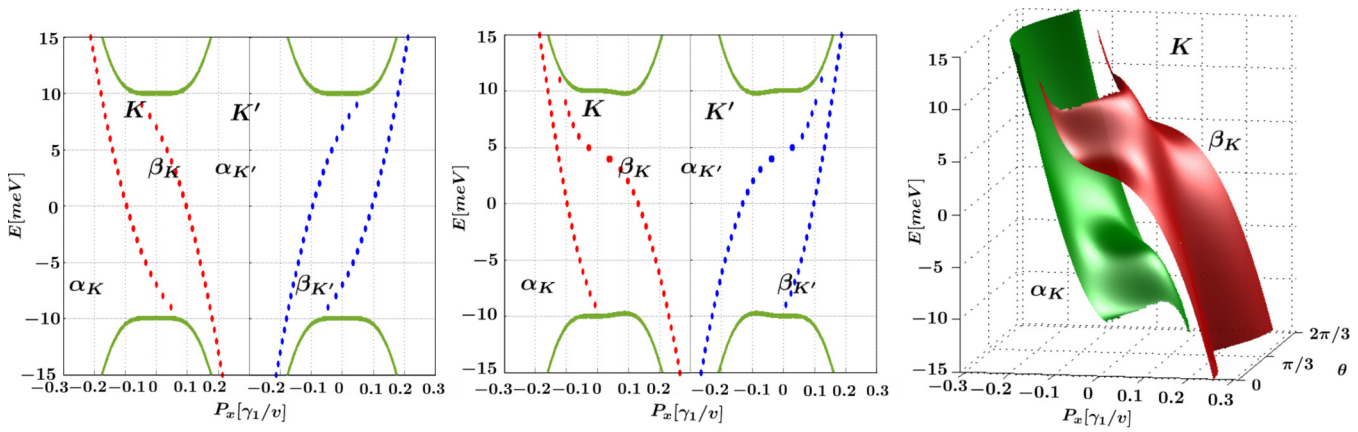

FIG. 2. (Color online) Topologically protected 1D modes. Left panel: modes in the absence of trigonal warping in the $\boldsymbol{K}$ (red) and $\boldsymbol{K'}$ (blue) valley, respectively; the low-energy conduction and valence bands are shown in green. Central panel: modes in the presence of trigonal warping with $\theta = 0$ in the $\boldsymbol{K}$ valley (red) and $\boldsymbol{K'}$ valley (blue); the low-energy conduction and valence bands are shown in green. Right panel: modulation of the 1D modes by the crystallographic orientation of the crystal, in the presence of trigonal warping in the $\boldsymbol{K}$ valley.

them with zeros and obtain a system of four equations,

$$\begin{pmatrix} T_{1,1} & T_{1,2} & 0 & 0 \\ T_{2,1} & T_{2,2} & 0 & 0 \\ T_{3,1} & T_{3,2} & -1 & 0 \\ T_{4,1} & T_{4,2} & 0 & -1 \end{pmatrix} \begin{pmatrix} A_1^+ \\ A_2^+ \\ A_3^- \\ A_4^- \end{pmatrix} = 0,$$

which only has a nontrivial solution if its determinant is equal to zero. Imposing the above condition, we reproduce the earlier results obtained by Ref. [7], namely that the band-gap interface confines the low-energy electron states along the interface, leading to the formation of two topologically protected 1D branches in the gapped region in each valley, as shown in Fig. 2 (left panel). Both branches in the $\boldsymbol{K}$ (red) valley, $\alpha_{\boldsymbol{K}}$ and $\beta_{\boldsymbol{K}}$, have negative group velocity at $E = 0$ whereas in the $\boldsymbol{K'}$ (blue) valley the branches $\alpha_{\boldsymbol{K'}}$ and $\beta_{\boldsymbol{K'}}$ have positive velocity. Note that this system is valley symmetric, and the branches in each valley can be obtained from the ones in the opposite valley by swapping the valleys and applying the electron-hole transformation $E \to -E$. Our results show that at low energies the $\alpha_{\boldsymbol{K}}$ and $\beta_{\boldsymbol{K'}}$ branches terminate on one end at $-u/2$, the top of the valence band, and continue throughout the conduction band. Oppositely, the $\beta_{\boldsymbol{K}}$ and $\alpha_{\boldsymbol{K'}}$ branches terminate on one end at $u/2$, bottom of the conduction band, and continue throughout the valence band. To test the upper/lower limits of the branches that continue throughout the bands, we repeat the above calculations using the four band model [19] and find that these branches terminate at $\pm\gamma_1$, respectively, where they merge with the bands.

Employing the same procedure as outlined above, we obtain the topologically protected channels in the presence of TrW, shown in Fig. 2 (central panel). Trigonal warping breaks the valley symmetry, and the branches in one valley can not be obtained from the ones in the opposite valley by applying the composite transformation discussed above, however, inversion symmetry is maintained. Moreover, as shown in Fig. 2 (right panel), the system possesses intravalley rotational symmetry by $2\pi/3$, and the crystallographic orientation of the crystal θ modulates the 1D branches. Referring back to the four band model [19], we checked that the branches which continue beyond $E = \pm u/2$ terminate at $E = \pm\gamma_1$.

Figure 3 shows the group velocity $v(\theta, E) = \partial E/\partial p_x$ and the inverse transverse confinement length $1/l(\theta, E) = \mathrm{Im}(p_y)/\hbar$ for the two branches in the $\boldsymbol{K}$ valley in Fig. 2 (right panel). Notice that the velocity and transverse confinement length are also modulated by the crystallographic orientation of the crystal. Similarly to a gapped parabolic spectrum, the group velocity for both branches is negative in the $\boldsymbol{K}$ valley, with their respective maxima being achieved at $\theta = 0$ and $2\pi/3$ or $\pi/3$ and at energies in the vicinity of the bands, and positive in the $\boldsymbol{K'}$ valley as dictated by time-inversion symmetry. The transverse confinement length follows the same pattern.

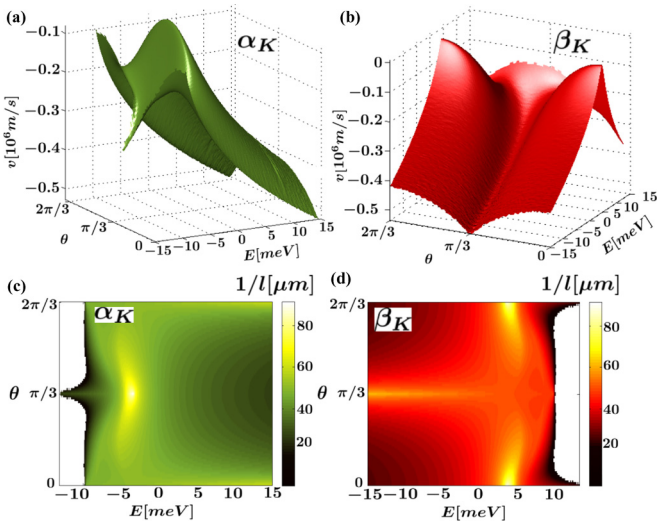

FIG. 3. (Color online) Group velocity (Top) and transverse confinement length (Bottom) of the topologically protected branches shown in Fig. 2 (Right panel). The colors differentiate between the $\alpha_{\boldsymbol{K}}$ (green) and $\beta_{\boldsymbol{K}}$ (red) branches.

IV. CONCLUSIONS

In conclusion, in trigonally warped bilayer graphene, an interface between regions with opposite bias polarity gives rise to two topologically confined states inside the gap which propagate along the interface in opposite directions in each valley. One of the chiral states starts at $E = -u/2$ and continues throughout the conduction band up to $+\gamma_1$, while the other starts at $E = +u/2$ and continues throughout the valence band down to $-\gamma_1$. Our analysis shows that while the direction of propagation of the two gapped states continues to be strictly determined by the valley, similarly to a gapped parabolic spectrum, both their group velocities as well as the transverse confinement lengths are now modulated by the crystallographic orientation of the crystal with respect to the interface.

ACKNOWLEDGMENTS

This project was funded by EC Graphene Flagship Project CNECTICT-604391, ERC Synergy Grant Hetero2D, Royal Society Wolfson Research Merit Award.

[1] M. Z. Hasan and C. L. Kane, Rev. Mod. Phys. **82**, 3045 (2010).
[2] X.-L. Qi and S.-C. Zhang, Rev. Mod. Phys. **83**, 1057 (2011).
[3] E. McCann and V. I. Fal'ko, Phys. Rev. Lett. **96**, 086805 (2006).
[4] F. Guinea, A. H. Castro Neto, and N. M. R. Peres, Phys. Rev. B **73**, 245426 (2006).
[5] E. McCann, Phys. Rev. B **74**, 161403 (2006).
[6] H. Min, B. Sahu, S. K. Banerjee, and A. H. MacDonald, Phys. Rev. B **75**, 155115 (2007).
[7] I. Martin, Y. M. Blanter, and A. F. Morpurgo, Phys. Rev. Lett. **100**, 036804 (2008).
[8] J. Martin, N. Akerman, G. Ulbricht, T. Lohmann, J. H. Smet, K. von Klitzing, and A. Yacoby, Nat. Phys. **4**, 144 (2008).

[9] A. Rycerz, J. Tworzydlo, and C. W. J. Beenakker, Nat. Phys. **3**, 172 (2007).

[10] P. San-Jose, E. Prada, E. McCann, and H. Schomerus, Phys. Rev. Lett. **102**, 247204 (2009).

[11] A. Varlet, M-H. Liu, V. Krueckl, D. Bischoff, P. Simonet, K. Watanabe, T. Taniguchi, K. Richter, K. Ensslin, and T. Ihn, Phys. Rev. Lett. **113**, 116601 (2014).

[12] K. S. Novoselov, E. McCann, S. V. Morozov, V. I. Fal'ko, M. I. Katsnelson, U. Zeitler, D. Jiang, F. Schedin, and A. K. Geim, Nat. Phys **2**, 177 (2006).

[13] J. D. Bernal, Proc. R. Soc. A **106**, 749 (1924).

[14] T. Ohta, A. Bostwick, T. Seyller, K. Horn, and E. Rotenberg, Science **313**, 951 (2006); J. B. Oostinga, H. B. Heersche, X. Liu, A. F. Morpurgo, and L. M. K. Vandersypen, Nat. Mater. **7**, 151 (2007); Y. Zhang, T.-T. Tang, C. Girit, Z. Hao, M. C. Martin, A. Zettl, M. F. Crommie, Y. R. Shen, and F. Wang, Nature (London) **459**, 820 (2009).

[15] E. V. Castro, K. S. Novoselov, S. V. Morozov, N. M. R. Peres, J. M. B. Lopes dos Santos, J. Nilsson, F. Guinea, A. K. Geim, A. H. Castro Neto, Phys. Rev. Lett. **99**, 216802 (2007).

[16] M. Mucha-Kruczynski, E. McCann, and Vladimir I. Falko, Semicond. Sci. Technol. **25**, 033001 (2010).

[17] Note that throughout this paper we assume $l \ll (\lambda_F, \sqrt{\frac{\hbar^2 v^2}{u\gamma_1}})$, where l is the width of the step and λ_F is the Fermi wavelength.

[18] Y. V. Nazarov and Y. M. Blanter, *Quantum transport: introduction to nanoscience* (Cambridge University Press, Cambridge, 2009).

[19] The electronic Hamiltonian for one valley in the basis $(\phi_{+,A_1},\phi_{+,B_2},\phi_{+,A_2},\phi_{+,B_1})^T$ in the $\boldsymbol{K}$ valley and $(\phi_{-,B_2},\phi_{-,A_1},\phi_{-,B_1},\phi_{-,A_2})^T$ in the $\boldsymbol{K}$ valley is $\hat{H} = \xi \begin{pmatrix} 0 & v_3\pi & 0 & v\pi^\dagger \\ v_3\pi^\dagger & 0 & v\pi & 0 \\ 0 & v\pi^\dagger & 0 & \xi\gamma_1 \\ v\pi & 0 & \xi\gamma_1 & 0 \end{pmatrix} - \eta \begin{pmatrix} 0 & \frac{v_3}{v}(\pi^\dagger)^2 & 0 & \pi^2 \\ \frac{v_3}{v}\pi^2 & 0 & (\pi^\dagger)^2 & 0 \\ 0 & \pi^2 & 0 & 0 \\ (\pi^\dagger)^2 & 0 & 0 & 0 \end{pmatrix}$. Here we assumed $a \ll l \ll (\hbar v/\gamma_1, \lambda_F)$, where a is the lattice constant, l is the width of the step and λ_F is the Fermi wavelength.